Journal of Global Positioning Systems (2009)
Vol.8, No.1 : 6-16

Journal of Global Positioning Systems
2009

Horizontal Strain Rate Distribution on an Active Ice Shelf Rift from in-situ GPS Data

Volker Janssen

Surveying and Spatial Sciences, School of Geography and Environmental Studies, University of Tasmania, Hobart, Australia.

Abstract

Mass loss from the Antarctic ice sheet predominantly occurs at the fringing ice shelves via iceberg calving, which is controlled by the initiation and propagation of large rifts that precede iceberg detachment and can lead to ice shelf break-up. This paper reports on the analysis of Global Positioning System (GPS) data collected at an active rift system on the Amery Ice Shelf, East Antarctica, over two field seasons. Horizontal strain rates are determined for a network of 11 sites observed over three weeks during the 2004/05 Antarctic summer period, and the results are combined with, and compared to, strain rates obtained in the 2002/03 season. Maximum principal strain rates across the network vary between 6 and 32 [x 10^{-3}/yr], while minimum principal strain rates are generally about 1-17 [x 10^{-3}/yr]. Changes evident in the strain distribution can mostly be attributed to existing fractures passing through the GPS network and the episodic movement of the rift tip. It is confirmed that rift propagation in 2005/06 was slowing down. Opening rates are inferred from baselines situated normal to the rift. Analysis of the network using a cumulative sum approach is found to be an effective method to detect small baseline length changes associated with rift propagation.

Keywords: GPS, strain, rift propagation, cumulative sum, Amery Ice Shelf

1 Introduction

Ice shelves are important components of the Antarctic ice sheet due to their ice-ocean-atmosphere interface and vulnerability to regional and global changes in atmospheric and oceanic temperatures (e.g. Mercer, 1978; Vaughan & Doake, 1996; Shepherd et al., 2004). The majority of mass lost from the Antarctic ice sheet takes place at the fringing ice shelves via iceberg calving, which accounts for up to 75% of the total loss (Jacobs et al., 1992). Iceberg calving is controlled by the initiation and propagation of large scale rifts (fractures that penetrate through the entire ice shelf thickness), which precede large tabular iceberg detachment and can lead to ice shelf break-up. These calving events are sporadic but occur in a natural cycle of advance and retreat of the ice shelf front with periods of typically several decades (Budd, 1966; Scambos et al., 2003). The retreat and disintegration of several ice shelves in the past few decades (e.g. Rott et al., 2002; De Angelis & Skvarca, 2003; Braun et al., 2009) has fuelled concern that these events could become more frequent in a warming climate. Furthermore, the very presence of ice shelves affects the continental flow of the grounded ice sheet towards the coast via the ice shelves by shielding these systems from a potential major retreat – this is known as the buttressing effect of ice shelves (Rignot et al., 2004).

In order to fully understand the processes contributing to the mechanics of ice shelf rift systems and how these may be affected by a changing climate, it is necessary to monitor such systems over an extended period of time. Over several Antarctic summer seasons between late 2002 and early 2006 an active rift system has been observed using a network of Global Positioning System (GPS) and seismic stations. This paper presents an analysis of the GPS measurements from the 2002/03 and 2004/05 field seasons, investigating strain distribution, propagation and widening of an active Antarctic ice shelf rift.

2 Study Area and Observations

The study area is the Amery Ice Shelf (AIS) in East Antarctica, which drains continental ice from an area of more than one million square kilometres (Allison, 1991) through a section of coastline that represents approximately 2% of the total continental circumference (Budd et al., 1967). Located at the front of the AIS, an

active rift system, known as the Loose Tooth, encompasses an area of about 30 km by 30 km that is expected to calve and produce a relatively large iceberg within the next decade (Fig 1). The last major calving event occurred in the Antarctic summer of 1963/64 when a ~10,000 km^2 iceberg detached from the ice shelf (Budd, 1966). Analysis of historical data mapping the ice shelf front suggests that a similar Loose-Tooth sized event preceded this major event (Fricker et al., 2002).

As depicted in Fig 1, the Loose Tooth consists of two longitudinal-to-flow rifts (denoted L1 and L2) which originated around 20 years ago and two transverse-to-flow rifts (denoted T1 and T2) which formed in 1995 (Bassis et al., 2007). In this region the ice shelf is ~400 m thick and the ice shelf flow is approximately 3 m/day (1.1 km/year) in a north-easterly direction (Bassis et al., 2005). The T2 tip was advancing at about 4 m/day during the period of late 1999 to early 2004, exhibiting a seasonal dependence with significantly higher rates in the summer period (Fricker et al., 2005b), however a slowing-down trend of rift propagation has recently been reported (Bassis et al., 2007). Evidence has been presented that rift propagation occurs in episodic bursts and is primarily driven by the internal glaciological stress of the ice shelf, rather than initiated by environmental factors such as wind speeds, tidal amplitudes or ocean swell (Bassis et al., 2005; 2008).

A GPS network of 11 sites (see Fig 1c), situated around the tip of the T2 rift and equipped with dual frequency GPS receivers, was observed over three weeks during the 2004/05 Antarctic summer period (Dec 18 – Jan 9). The GPS antennae were set up on 2.3-metre long aluminium poles that were rammed into the ice as far as possible. It should be noted that the actual observation span was longer, but due to gradual tilting of the poles caused by melting in the second half of the field season only the first three weeks of data were utilised in this study. The receivers were powered by batteries and solar panels, and a sampling rate of 30 seconds was utilised. GPS data were processed in daily (24-hr) sessions with the Leica Geo Office version 5.0 software, using IGS precise ephemerides and full (relative) antenna phase centre variation models at all sites. The Saastamoinen model was applied to account for the tropospheric delay, while an ionosphere model was computed from the reference station data of each baseline.

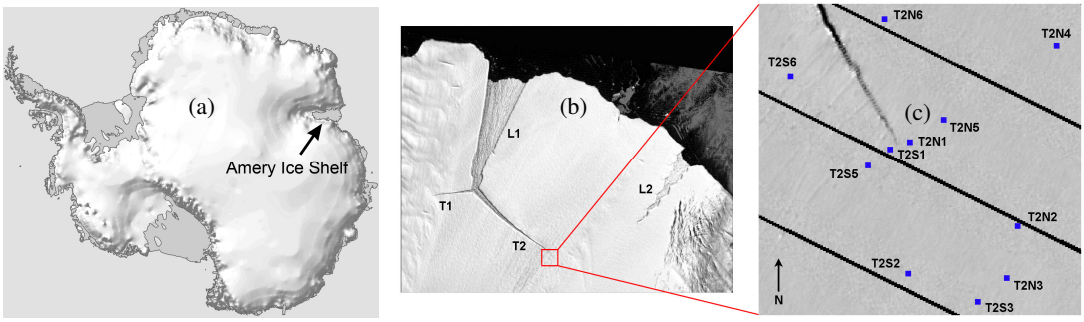

Fig. 1: (a) Amery Ice Shelf (image courtesy of Australian Antarctic Data Centre), (b) Landsat-7 ETM+ image of the Loose Tooth rift system acquired on March 2, 2003, and (c) location of GPS stations around the tip of T2 overlaid on a Landsat-7 image acquired on January 9, 2005. The regular pattern of black lines visible represents data gaps caused by the failure of the SLC (Scan Line Corrector) module in the ETM+ sensor on the Landsat-7 satellite, which occurred on May 31, 2003 (USGS, 2009).

3 Strain Analysis

Since the distances between sites are short (< 1.5 km) and relative measurements between points are used, a quasi-stationary ice shelf can be assumed where differential tidal motion and atmospheric variations between sites are assumed negligible, i.e. common systematic effects are removed. In fact, in this region the ice shelf experiences horizontal movement of about 3 m/day in a north-easterly direction (Young & Hyland, 2002; Bassis et al., 2005) and a vertical, tidal motion with a peak-to-peak amplitude of approximately 1-2 m (King et al., 2000; Zhang & Andersen, 2006). It is recognised that unmodelled tidal signals have the potential to bias results in unexpected ways (King, 2004). However, because the size of the network is small compared to the wavelength of the tide, the differential motion due to the tide between sites is insignificant (less than mm over the network using the CATS02.01 tide model generated by Padman et al. (2002)). With the underlying uniform motion of the ice shelf across the network removed, any remaining relative movements between network points can be interpreted as strain.

Baseline processing produced a set of daily baselines in terms of International Terrestrial Reference Frame 2000 (ITRF2000) (Altamimi et al., 2002) global Cartesian coordinate differences, which were transformed into a local north-east-up (NEU) coordinate system and aligned (rotated) with the local flow direction of the AIS. It should be noted that over these short distances the effect of earth curvature is not significant and can therefore be ignored. AUSPOS (2007) processing of the entire dataset in daily (24-hr) sessions was utilised to determine the local flow direction of 48.6° ± 0.6°, which, in this case, is predominantly orthogonal to the rift propagation

direction. CSRS-PPP (2008) processing confirmed these values. The GPS network was tessellated into individual triangles, and strain rates were then determined according to the procedure outlined by Brunner et al. (1981).

Table 1 lists the strain parameters determined. ε_{xx} and ε_{yy} are the extensions in the x and y directions respectively, and ε_{xy} is the shear strain component (negative values indicate compression). In this study, the x axis represents the longitudinal-to-flow (i.e. normal-to-rift) direction while the y axis refers to the transverse-to-flow (i.e. parallel-to-rift) direction. γ_1 and γ_2 are the widely used engineering shear strains, and γ_{max} is the maximum shear strain. e_{max} and e_{min} represent the maximum and minimum principal strains, respectively, and α_{max} is the azimuth of the maximum principal strain, oriented to true north.

Maximum principal strain rates are of the order of 6-32 [x 10^{-3}/yr] across the network, with two extremes of 87 and 97 [x 10^{-3}/yr] in the two 'sliver' triangles S1-N1-N2 and S1-N6-N1, respectively, which are anchored on both sides of the rift tip and include the short across-rift tip baseline T2S1-T2N1. Minimum principal strain rates are generally about 1-17 [x 10^{-3}/yr]. The orientation axes and magnitudes of the principal strain rates within the network are illustrated in Fig 2.

Transverse-to-flow strain rates generally exceed longitudinal-to-flow strain rates, with the obvious exception of the two 'sliver' triangles and the triangle behind the rift tip (S1-S6-N6). The dominance of longitudinal-to-flow strain rates in these triangles may be explained by rift widening at and behind the rift tip. In contrast, transverse-to-flow strain rates dominate in front of the rift tip since the rift has not yet penetrated that far.

These findings are in agreement with results obtained during the following 2005/06 Antarctic summer season, where an almost identical network configuration but a different data processing methodology was used to determine maximum principal strain rates of about 11-25 [x 10^{-3}/yr] with extremes of 71 [x 10^{-3}/yr] and minimum principal strain rates of 4-11 [x 10^{-3}/yr] (Bassis et al., 2007).

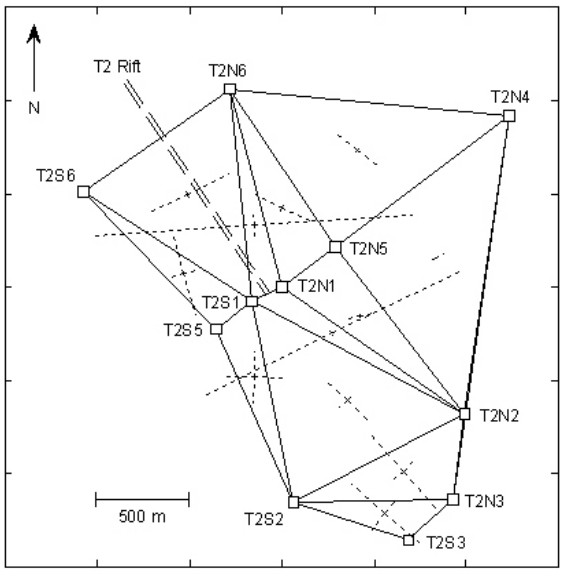

Fig. 2: Strain distribution, based on all observations (2004/05).

Table 1: Mean strain rates determined for each triangle based on all observations.

Triangle / Parameter	N5-N4-N2 [10^{-3}/yr]	N1-N5-N2 [10^{-3}/yr]	S1-N1-N2 [10^{-3}/yr]	S1-N2-S2 [10^{-3}/yr]	S2-N2-N3 [10^{-3}/yr]	S2-N3-S3 [10^{-3}/yr]
ε_{xx}	5.3 ± 0.1	6.1 ± 0.1	87.7 ± 0.4	7.0 ± 0.1	8.5 ± 0.1	14.1 ± 0.1
ε_{yy}	1.3 ± 0.1	1.5 ± 0.1	-13.2 ± 0.2	18.1 ± 0.1	31.7 ± 0.1	27.4 ± 0.2
ε_{xy}	1.2 ± 0.1	3.7 ± 0.1	28.3 ± 0.3	0.8 ± 0.1	0.1 ± 0.1	2.0 ± 0.1
γ_1	-4.0 ± 0.1	-4.5 ± 0.1	-91.9 ± 0.4	11.1 ± 0.1	23.2 ± 0.1	13.3 ± 0.2
γ_2	2.4 ± 0.1	7.3 ± 0.2	56.5 ± 0.7	1.5 ± 0.1	0.2 ± 0.1	4.0 ± 0.2
γ_{max}	4.7 ± 0.1	8.6 ± 0.1	107.9 ± 0.5	11.2 ± 0.1	23.2 ± 0.1	13.9 ± 0.2
e_{max}	5.6 ± 0.1	8.1 ± 0.1	86.7 ± 0.3	18.2 ± 0.1	31.7 ± 0.1	27.7 ± 0.1
e_{min}	1.0 ± 0.1	-0.5 ± 0.1	-21.2 ± 0.3	6.9 ± 0.1	8.5 ± 0.1	13.8 ± 0.1
α_{max}	64.1° ± 0.4°	77.7° ± 0.3°	64.4° ± 0.2°	134.7° ± 0.2°	138.4° ± 0.1°	130.2° ± 0.5°

Triangle / Parameter	S5-S1-S2 [10^{-3}/yr]	S5-S6-S1 [10^{-3}/yr]	S1-S6-N6 [10^{-3}/yr]	S1-N6-N1 [10^{-3}/yr]	N1-N6-N5 [10^{-3}/yr]	N5-N6-N4 [10^{-3}/yr]
ε_{xx}	-1.6 ± 0.1	-1.9 ± 0.1	26.3 ± 0.1	62.8 ± 0.2	5.9 ± 0.1	3.0 ± 0.1
ε_{yy}	0.7 ± 0.1	19.6 ± 0.1	5.4 ± 0.1	40.2 ± 0.2	16.6 ± 0.1	15.9 ± 0.1
ε_{xy}	-16.8 ± 0.1	-13.6 ± 0.1	6.0 ± 0.1	43.7 ± 0.2	5.5 ± 0.1	2.6 ± 0.1
γ_1	2.3 ± 0.2	21.4 ± 0.1	-20.9 ± 0.1	-22.6 ± 0.3	10.7 ± 0.1	12.9 ± 0.1
γ_2	-33.7 ± 0.3	-27.3 ± 0.3	11.9 ± 0.1	87.5 ± 0.4	10.9 ± 0.1	5.1 ± 0.1
γ_{max}	33.7 ± 0.3	34.7 ± 0.2	24.0 ± 0.1	90.3 ± 0.4	15.3 ± 0.1	13.9 ± 0.1
e_{max}	16.4 ± 0.1	26.2 ± 0.1	27.8 ± 0.1	96.7 ± 0.2	18.9 ± 0.1	16.3 ± 0.1
e_{min}	-17.3 ± 0.1	-8.5 ± 0.1	3.8 ± 0.1	6.4 ± 0.2	3.6 ± 0.1	2.5 ± 0.1
α_{max}	181.7° ± 0.1°	164.5° ± 0.2°	63.5° ± 0.1°	86.4° ± 0.1°	115.8° ± 0.2°	127.8° ± 0.2°

It is recognised that the two 'sliver' triangles are geometrically weak which may negatively affect the reliability of the calculated strain rates. However, it should be noted that the triangles S5-S6-S1 and S5-S1-S2

(located entirely on the southern side of the rift) exhibit a very similar geometry but do not produce such extreme values, indicating that the results are sufficiently reliable for the purposes of this study.

Earlier studies based on terrestrial observations in the 1960s (Budd, 1966; Budd et al., 1982), later reanalysed by King (2002) in combination with GPS data, and based on InSAR analysis (Young & Hyland, 2002) reported longitudinal strain rates (ε_{xx}) of 6-8 [x 10^{-3}/yr] and transverse strain rates (ε_{yy}) of 4-8 [x 10^{-3}/yr] towards the ice shelf front. These values agree only in part with the results presented here since they do not consider the dynamics in close proximity to a propagating ice shelf rift. However, Young & Hyland (2002) also noted that transverse strain rates begin to exceed longitudinal strain rates at the front of the ice shelf and stated a transverse strain rate of 40 [x 10^{-3}/yr] for the vicinity of the L1 rift on the Loose Tooth.

3.1 Short-term Changes in Strain Distribution

In order to investigate any short-term changes in strain rates, the baseline length observations were arranged into 4-day bins. This bin size was chosen to ensure a sufficient number of observations while decreasing the noise level and accommodating the fact that jumps in baseline length caused by the periodic nature of rift propagation last approximately 2-4 hours and are generally separated by 10-20 days (Bassis et al., 2007). Analysis of the results shows that changes in strain rate distribution are evident both through variations in axis orientation and in magnitude over the observation period (Fig 3).

It should be noted that the uncertainties associated with the determined strain rates are below 0.4 [x 10^{-3}/yr], while the azimuths exhibit uncertainties of below 1°, in a few isolated cases reaching almost 2°. Large variations in strain rates are evident around day 9 for most of the triangles including at least one of the two sites located closest to the rift tip (T2S1 and T2N1). The largest change appears in those triangles including the across-rift tip baseline between these two points, i.e. the two 'sliver' triangles. These two triangles and the two triangles S5-S6-S1 and S5-S1-S2, located on the southern side of the rift, show significant changes in strain rate distribution. The strain rates double in magnitude, while a clockwise rotation of up to 30° is evident, suggesting that these two parameters are related (Fig 4). Triangle S1-N2-S2, situated immediately in front of the rift tip, exhibits a similar behaviour (Fig 5b).

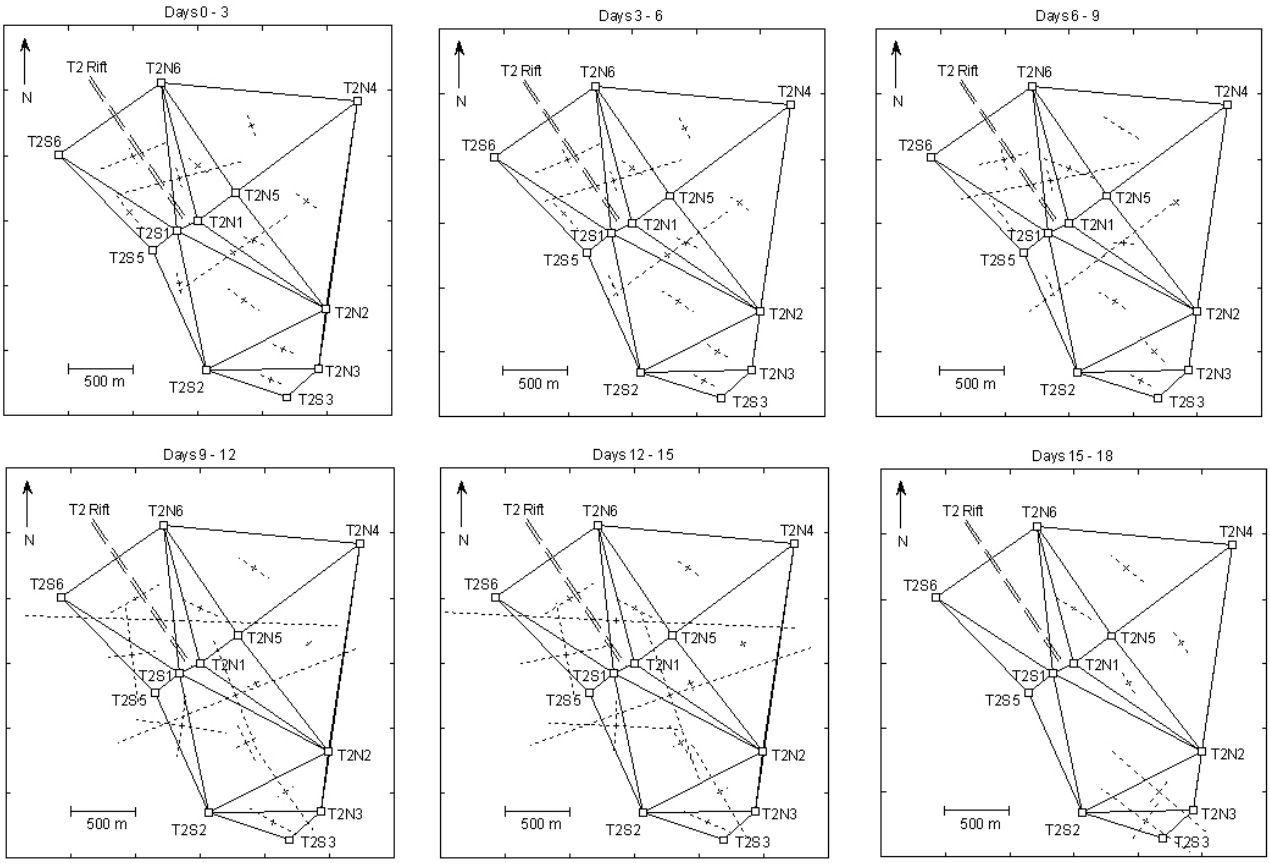

Fig. 3: Changes in strain distribution using 4-day bins. Day numbers are relative to the start of processing (Dec 18, 2004), i.e. day 1 corresponds to Dec 19, etc.

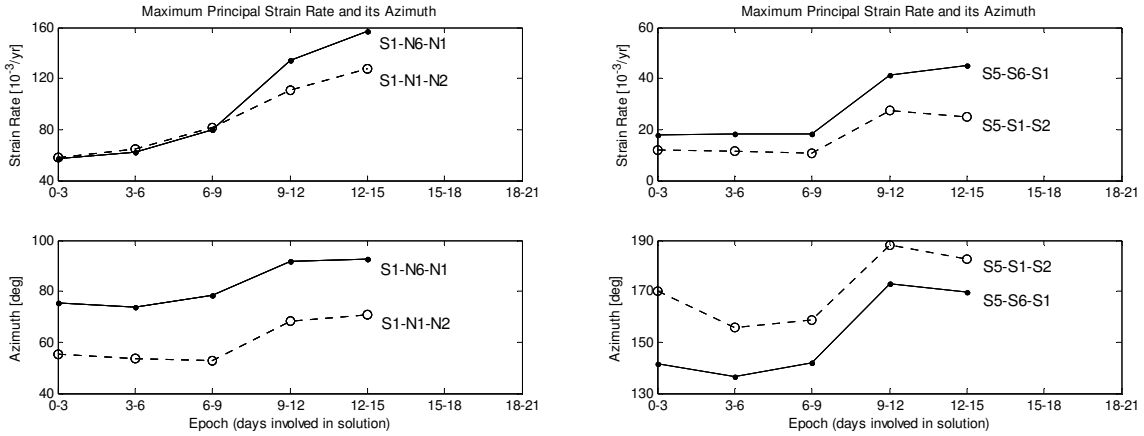

Fig. 4: Changes in maximum principal strain rate and its azimuth for (a) the 'sliver' triangles S1-N6-N1 and S1-N1-N2 and (b) the triangles S5-S6-S1 and S5-S1-S2 on the southern side of the rift.

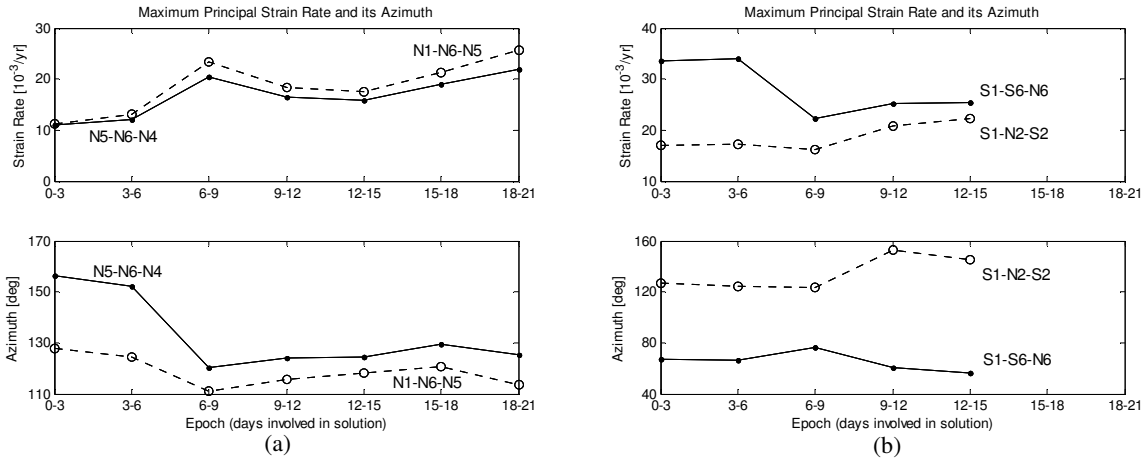

Fig. 5: Changes in maximum principal strain rate and its azimuth for triangles (a) N5-N6-N4 and N1-N6-N5 (behind rift tip on northern side) and (b) S1-S6-N6 and S1-N2-S2 (immediately behind and in front of rift tip).

The apparent jump neatly coincides with a burst in rift propagation on 27 December 2004, i.e. day 9 in the time series used in the present study, detected by seismic observations at the network sites (Bassis et al., 2007). Strain rates computed using data from either side of the period of the jump are comparatively similar, supporting the conclusion that this jump in rift propagation caused these changes. Smaller changes in strain distribution are evident throughout the network and can most likely be attributed to the movement of existing longitudinal-to-flow fractures, spaced about 300-400 m apart (see Fig 1).

Further evidence for a link between changes in the maximum principal strain rate and its direction is presented by the two triangles located behind the rift tip on the northern side of the rift, which exhibit a distinct change around day 6 (Fig 5a). It is unlikely that this activity is related to the burst in rift propagation on day 9, rather it is suggested that these changes are caused by the existence of several longitudinal-to-flow fractures (see Fig 1c), showing the dynamics of a complex active ice shelf rift system.

Exceptionally large strain rate variations are also evident in the two triangles S2-N2-N3 and S2-N3-S3, both located more than a kilometre in front of the rift tip. An increase in the maximum principal strain rate from 13 to 58 [x 10^{-3}/yr] and from 12 to 40 [x 10^{-3}/yr] is evident over the observation period, while the relating azimuths increase by 30° and 40° respectively (Fig 6a). The strain rate in triangle S2-N2-N3 shows a jump around day 9, while a similar jump is visible about 6 days later in triangle S2-N3-S3. This behaviour makes sense in terms of rift propagation since the latter triangle is situated further ahead of the rift. However, the distance between the triangle centroids is 250 m, or 105 m in the direction of the rift, while the rift appears to have only propagated 13 m during these 6 days (calculated by fitting a function to observations of rift positions since 1999). Hence, it is not conclusive whether this activity is linked to the burst in rift propagation on day 9 or caused by other factors such as micro-cracks in front of the rift tip.

In regards to particularly large changes in the direction of the maximum principal strain rates, triangles N5-N4-N2

and N1-N5-N2, both located in front of the rift tip on the northern side of the rift, show a substantial decrease in azimuth of 70° and 50° respectively. In both cases this anti-clockwise rotation coincides with the maximum principal strain rate being reduced to half its value in the same time period (Fig 6b). The reason for this behaviour currently remains unknown.

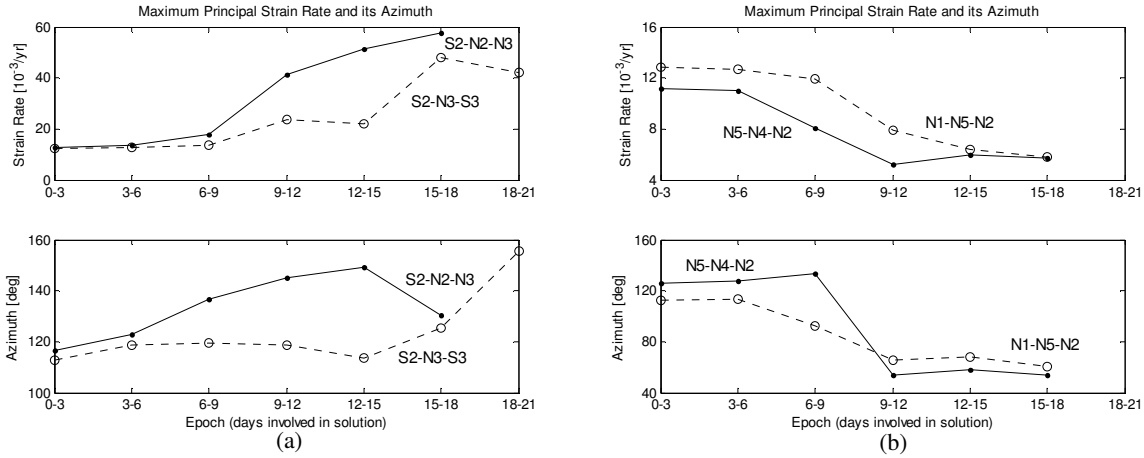

Fig. 6: Changes in maximum principal strain rate and its azimuth for triangles (a) S2-N2-N3 and S2-N3-S3 (in front of rift tip) and (b) N5-N4-N2 and N1-N5-N2 (in front of rift tip on northern side).

3.2 Changes in Strain Distribution between Field Seasons

In order to investigate possible changes in rift fracture mechanics between field seasons, the 2004/05 results are aligned with, and compared to, strain rates obtained in the earlier 2002/03 Antarctic summer season, when a sparser 6-station network with baselines < 5 km was deployed for 46 days (Dec 8 – Jan 23). Maximum principal strain rates were of the order of 12-21 [x 10^{-3}/yr] across the 2002/03 network, while minimum principal strain rates were approximately 2-9 [x 10^{-3}/yr] (Janssen et al., 2009), generally smaller than in the later season. Analysis of the 2002/03 data showed that transverse-to-flow strain rates generally exceeded longitudinal-to-flow strain rates, with the exception of a balanced situation occurring in front of the rift tip. Maximum principal strain rates were generally smaller in front of the tip, compared to the situation on either side of the rift.

Considering ice shelf flow and rift propagation between these two field seasons, both networks are referenced to the rift tip (Fig 7), however, obviously referring to different parts of the ice shelf. In the latter season the rift tip is located closer to a suture zone formed by two ice streams merging upstream. Mean values for ice velocity and flow direction were determined based on the 2002/03 and 2004/05 datasets (3.1 m/day and 46° respectively) and applied to the 2002/03 positions to align both networks.

In both seasons, and in agreement with the 2005/06 results reported by Bassis et al. (2007), triangles spanning the rift are generally characterised by maximum principal strain axes aligned normal to the rift (approximately longitudinal-to-flow), while triangles anchored entirely on one side of the rift generally exhibit maximum principal strain rates aligned parallel to the rift (approximately transverse-to-flow) (see Fig 7). This indicates that longitudinal-to-flow strain can be largely accounted for by rift opening. A rotation in the direction of the maximum principal strain is evident around the rift tip, which may be related to the rotation of the Loose Tooth as a whole as the T2 rift lengthens/widens and the L1 rift widens.

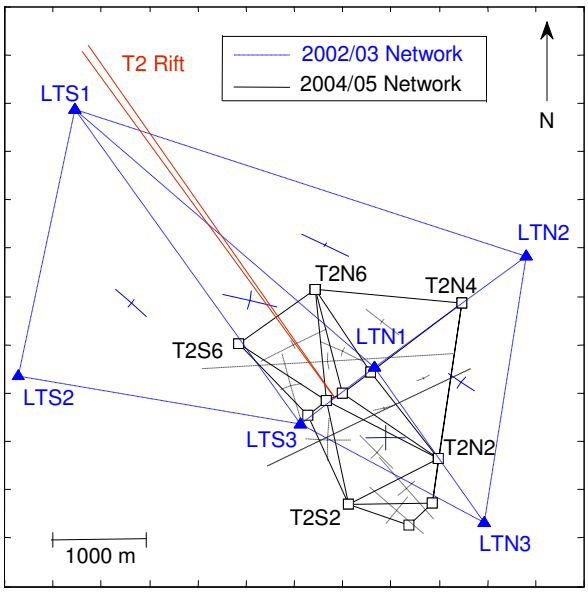

Fig 7: 2002/03 and 2004/05 networks aligned relative to the rift tip.

4 Rift Propagation and Opening Rates

The 2002/03 rift tip coordinates were shifted into the 2004/05 system by applying the mean values for ice shelf velocity and flow direction mentioned above. It was determined that the rift propagated ~1 km in the two years between the field seasons discussed here, less than the previously reported rate of ~1.5 km/yr (Fricker et al., 2005b), suggesting a slowing down of rift propagation. Further evidence for this slowing-down trend has recently been presented and accredited to either the rift propagating through existing fractures and shear bands within a suture zone (formed by two ice streams merging upstream) which causes a decrease in stress at the rift tip or the rift propagating into a thicker band of marine ice (Bassis et al., 2007).

The analysis of baseline distances situated normal to the rift can be used to infer opening rates of the rift as the rift tip passes through the GPS network. In the 2004/05 season, the shortest baseline spanning the rift, T2S1-T2N1 (170 m), increases in baseline length initially by approximately 30 mm/day and exhibits one jump of ~20 mm between days 8 and 9 (Fig 8a), corresponding to a known jump on day 9 inferred from seismic data collected at the sites (Bassis et al., 2007). Following this jump, a much higher opening rate of ~50-60 mm/day is evident. This behaviour is supported by the longer (526 m) baseline T2N5-T2S1 (Fig 8b), although it should be noted that this observation is based on only 16 days of GPS data and should therefore be treated with caution.

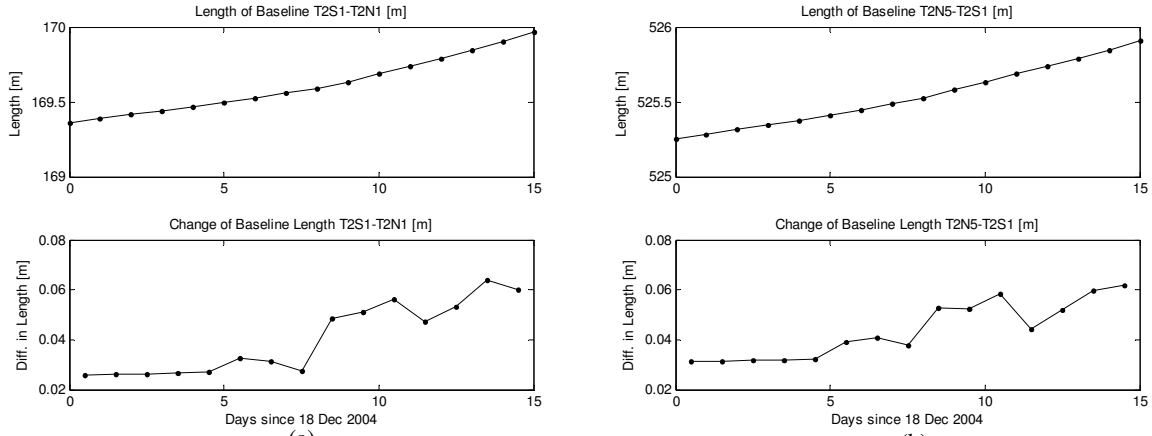

Fig. 8: Time series of baseline length and first differences: (a) T2S1-T2N1 and (b) T2N5-T2S1. Day numbers are relative to the start of processing.

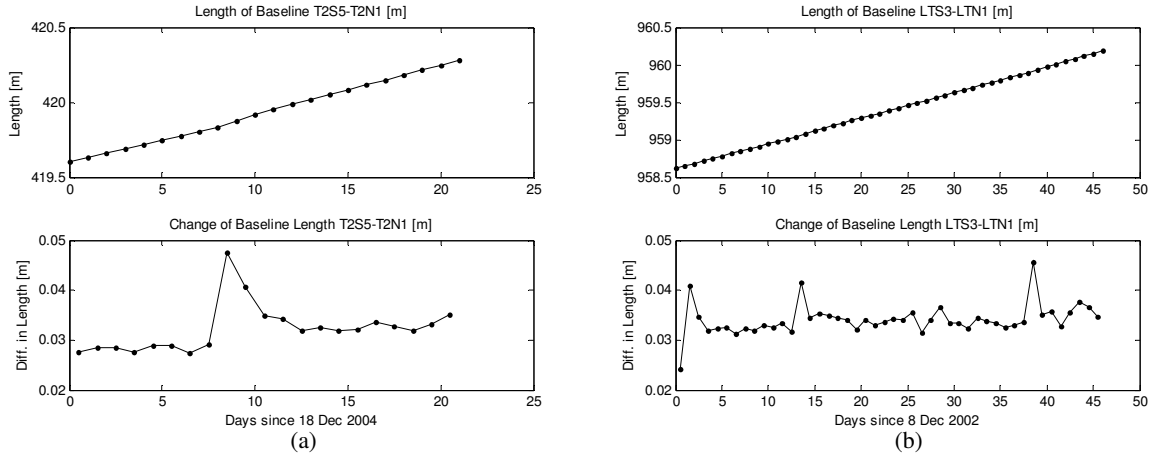

Fig. 9: Time series of baseline length and first differences: (a) T2S5-T2N1 (2004/05) and (b) LTS3-LTN1 (2002/03).

The third across-rift tip baseline, T2S5-T2N1 (420 m), was observed for a longer time period and, although confirming the initial opening rate of ~30 mm/day as well as the location and magnitude of the jump, does not show a similar increase in the opening rate (Fig 9a). Instead, the opening rate is slightly lower than 30 mm/day before and slightly higher after the jump occurs, exhibiting an increase of only ~5 mm/day. This behaviour of the opening rate compares well to the findings of the 2002/03 season (Fig 9b) where, based on a baseline of 960 m length, a consistent opening rate across the rift tip of ~35 mm/day was determined while three jumps with a magnitude of ~10 mm were identified (Bassis et al., 2005; Janssen et al., 2009). A consistent jump magnitude of ~10 mm was also reported for the 2005/06 season (Bassis et al., 2007).

The increase in the magnitude of the detected jump is therefore at odds with findings from the earlier and later field seasons. Since the dataset used in this study contains only one jump, it is impossible to determine whether this individual jump is exceptionally large or whether this behaviour extends across the entire summer season. As evident from automatic weather station (AWS) data collected at G3, located on the Amery Ice Shelf about 240 km south of the Loose Tooth, the Antarctic summer of 2004/05 was comparatively warm in the region (Fig 10) with maximum daily temperatures reaching up to +8°C during the observation period. This may suggest a link to the higher jump magnitude. However, it should be noted that, due to the complexity of the rifting process, higher temperatures do not directly translate into more active rifting (Bassis et al., 2008).

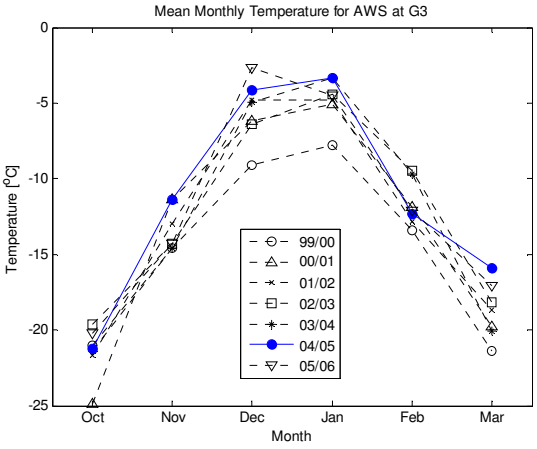

Fig. 10: Average monthly temperature on the Amery Ice Shelf for several summer seasons.

Two baselines straddling the rift ~1 km behind and ~1 km in front of the rift tip were also investigated. Behind the rift tip, a significant decrease in opening rate from ~90 mm/day to ~10 mm/day, paired with the existence of two possible jumps, is evident during the observation span (Fig 11a), suggesting that the widening of the rift undergoes substantial variation long after the rift tip has travelled through this area. In this case, a general trend of the rift opening slowing down to zero is visible, however, a longer dataset is needed in order to investigate how long this apparent period of near-zero opening may last. As seen in Fig 1c, large longitudinal-to-flow fractures are present across this baseline, most likely causing these changes in combination with material falling into the rift and possibly wedging it open.

In front of the rift tip, a relatively steady baseline length extension of ~25 mm/day is evident, again exhibiting possible jumps that may be attributed to longitudinal-to-flow fracture activity (Fig 11b). However, one of these jumps is uncharacteristically large with a magnitude of >60 mm and needs to be treated with caution. In the absence of a longer time series it cannot be determined whether this is in fact genuine rifting activity or an outlier caused, for example, by increased noise and/or adverse ionospheric conditions in the second half of the observation period over this comparatively long baseline in the network.

Based on MODIS and ICESat data collected in proximity to the rift tip, Fricker et al. (2005a) calculated a longer-term opening rate of 18 m/yr (~50 mm/day), which agrees to a certain extent with the results presented here. These opening rates are an order of magnitude smaller than those present in rifts on the Ross Ice Shelf (150-250 m/yr), as inferred from SAR imagery by Joughin & MacAyeal (2005). However, it is important to note that the GPS-derived rates presented here are determined at the rift tip where rift opening is smallest. In addition, GPS observations provide a direct measurement of rift opening while ICESat and SAR results are inferred from other observations. A dataset including several across-rift GPS baselines, evenly distributed along the rift, is needed in order to make more detailed statements about the short-term behaviour of opening rates in proximity to the rift tip.

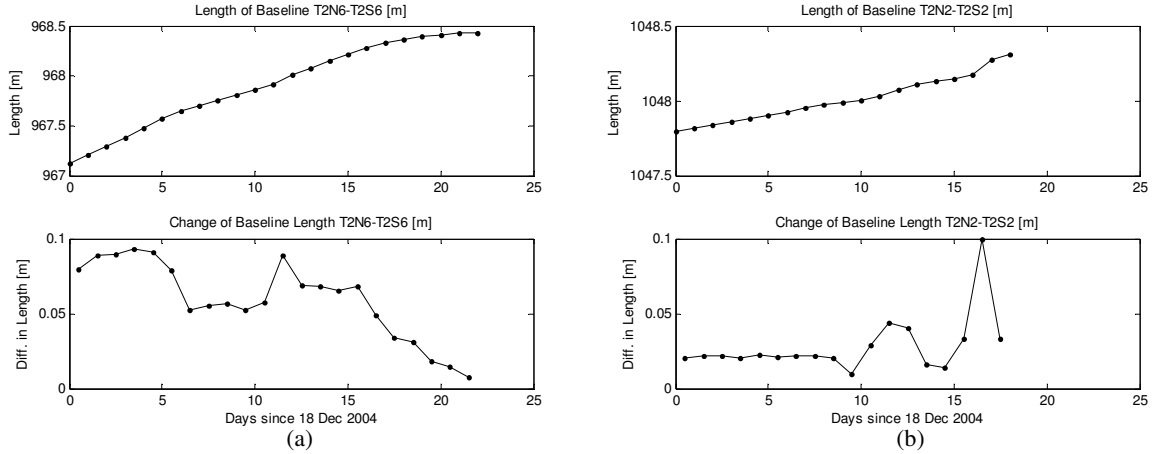

Fig. 11: Time series of baseline length and first differences: (a) T2N6-T2S6 (behind the rift tip) and (b) T2N2-T2S2 (in front of the rift tip).

5 Cumulative Sum Analysis

Cumulative sum (CUSUM) charts are a graphical method of change point detection and can be used to reveal subtle changes in baseline time series (Iz, 2006). Forming the difference of two baselines that share a common site reduces common systematic errors and thereby allows the detection of small changes with better signal-to-noise ratios. If the two baselines run approximately parallel and perpendicular to the expected deformation, subtle baseline changes remain in the differenced residuals, although their magnitude will be reduced as any common signal is removed in the difference, and thus can be detected.

In practice, after removing any linear trends and periodic variations from the baseline length time series, the resulting residuals are used as quasi-observations for further analysis. Any sudden change in the slope of the CUSUM indicates a shift in the mean, i.e. a jump in the baseline length.

Several scenarios anticipated in a deformation monitoring situation were investigated by simulation of baseline time series, including a uniform linear trend in baseline length, a change of the linear trend in a particular epoch, a change of the linear trend including a jump in baseline length (i.e. the situation experienced at a propagating rift tip), a linear trend changing to a constant baseline length, a linear increase-then-decrease situation, and a jump with constant baseline lengths on either side (Fig 12a). In this simulation, a change was introduced between epochs 13 and 14, indicated in Fig 12 by a vertical line at epoch 13.

If the original baseline lengths are used as input, as proposed by Iz (2006), sudden changes in the time series generally appear as change points of sinusoidal-like curves in the resulting CUSUM charts, making identification not obvious. If the technique is modified in order to use first differences (between successive epochs) as input rather than the original baseline lengths (Janssen, 2009), any sudden change can easily be detected as a clear peak or jump (Fig 12b).

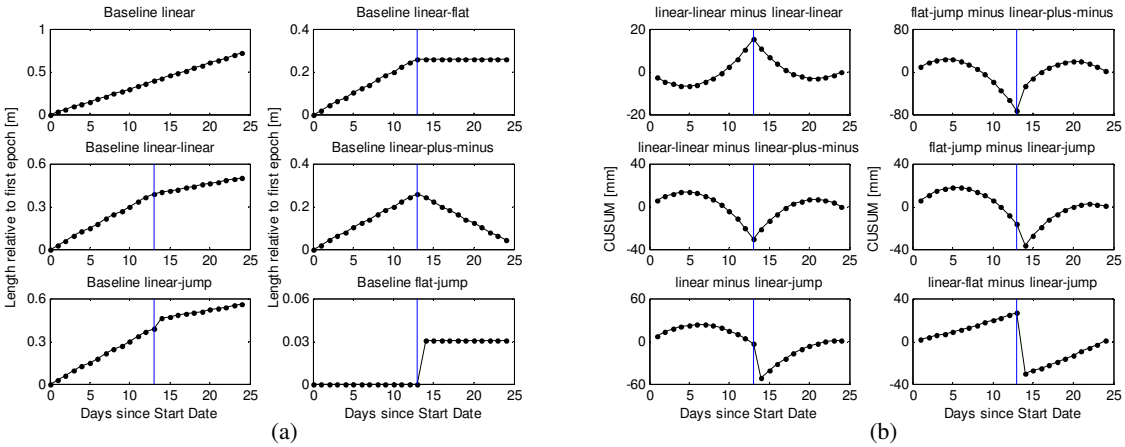

Fig. 12: CUSUM simulation: (a) cases investigated and (b) selected results. The vertical line indicates the epoch in which a change was introduced.

Several baseline pairs of the 2004/05 Loose Tooth GPS network were analysed using this CUSUM technique. A known jump in baseline length across the rift tip on day 9, inferred from seismic data collected at the sites (Bassis et al., 2007), can be reliably detected as a peak on day 8 in all pairs containing an across-rift tip baseline (Fig 13). Only in one pair, as seen in the upper-right panel, the peak is masked somewhat. These results show that the CUSUM technique is an effective method to detect small baseline length changes and can therefore be very useful in the identification of jumps in rift propagation. Other peaks are visible, possibly attributable to fractional movements in longitudinal flow lines and across-rift jumps, but at this stage no conclusive statement can be made due to the limited number of baseline pairs available. In order for a jump to be reliably determined, it needs to be present in multiple baseline pairs.

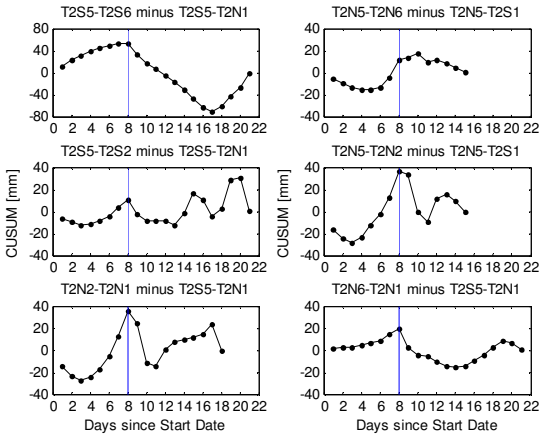

Fig. 13: CUSUM results (2004/05).

6 Conclusions

The distribution of horizontal strain rates in close proximity to the tip of a propagating rift system on the Amery Ice Shelf, East Antarctica has been determined using in-situ GPS observations. In the 2004/05 field season, maximum principal strain rates are of the order of 6-32 [x 10^{-3}/yr] across the network, while minimum principal strain rates are generally about 1-17 [x 10^{-3}/yr]. Triangles spanning the rift exhibit maximum principal strain axes aligned normal to the rift (approximately longitudinal-to-flow), while triangles anchored entirely on one side of the rift are generally characterised by maximum principal strain rates aligned parallel to the rift (approximately transverse-to-flow). This indicates that longitudinal-to-flow strain can be largely accounted for by rift opening. Evident short-term changes in the strain distribution can mostly be attributed to the GPS baselines straddling existing longitudinal-to-flow fractures and the episodic movement of the rift tip. A rotation in the direction of the maximum principal strain is evident around the rift tip, which may be related to the rotation of the Loose Tooth as a whole in response to the T2 rift lengthening/widening and the L1 rift widening, as previously suggested by Bassis et al. (2007).

A comparison of the mean GPS coordinates of the rift tip obtained in both field seasons, under consideration of a mean ice flow direction and velocity, confirmed the trend that the T2 rift propagation is currently decreasing. The rift only propagated ~1 km in two years, between the Antarctic summer seasons of 2002/03 and 2004/05. Across the rift tip, it was found that opening rates increased significantly after a jump in the baseline length occurred, rather than at once returning back to their previous level. In addition, a jump magnitude of 20 mm was determined, i.e. 10 mm larger in comparison to earlier and later field seasons. Since the dataset used in this study contains only one jump, it was not possible to determine whether this individual jump is exceptionally large or whether this behaviour extends across the entire summer season. Automatic weather station (AWS) data collected on the AIS shows that the 2004/05 field season was comparatively warm, which may suggest a link to the higher jump magnitude and accelerated opening rates. However, due to the complexity of the rifting process, higher temperatures do not directly translate into more active rifting. In this context, it should also be noted that each field campaign only provides a snapshot of the actual dynamics at the rift tip, and continuous measurements (ideally over an entire year) are needed to fully monitor its propagation.

Analysis of the GPS network using a cumulative sum (CUSUM) approach, obtained by differencing a pair of residual baseline time series situated approximately normal and parallel to the rift, is found to be an effective method to detect small baseline length changes associated with rift propagation. Simulation shows that using first differences (between successive epochs) as input produces clear peaks or jumps in the CUSUM time series when a sudden change in baseline length occurs. This is confirmed by the results obtained from the 2004/05 GPS data, reliably identifying a known jump in the baseline length time series.

Acknowledgements

GPS data collection was supported by the Australian Government Antarctic Division through Australian Antarctic Science grants to Prof. Richard Coleman who is gratefully acknowledged for providing these data and invaluable advice during the course of this study. Work at the University of Tasmania was supported by an IRGS grant to the author. Satellite imagery was kindly provided by Neal Young (Antarctic CRC and Australian Government Antarctic Division), and AWS data was sourced from the Australian Government Antarctic Division Glaciology Program.

References

Allison, I. (1991), ***The Lambert Glacier/Amery Ice Shelf study: 1988-1991***, *Aurora*, vol. 10, no. 4, pp. 22-25.

Altamimi, Z., Sillard, P. and Boucher, C. (2002), ***ITRF2000: A new release of the International Terrestrial Reference Frame for earth science applications***, *Journal of Geophysical Research*, vol. 107, no. B10, 2214, doi:10.1029/2001JB000561.

AUSPOS (2007), ***Online GPS processing service***, http://www.ga.gov.au/geodesy/sgc/wwwgps/ (accessed July 21, 2009).

Bassis, J.N., Coleman, R., Fricker, H.A. and Minster, J.B. (2005), ***Episodic propagation of a rift on the Amery Ice Shelf, East Antarctica***, *Geophysical Research Letters*, vol. 32, no. 2, L06502, doi:10.1029/2004GL022048.

Bassis, J.N., Fricker, H.A., Coleman, R., Bock, Y., Behrens, J., Darnell, D., Okal, M. and Minster, J.B. (2007), ***Seismicity and deformation associated with ice-shelf rift propagation***, *Journal of Glaciology*, vol. 53, no. 183, pp. 523-536.

Bassis, J.N., Fricker, H.A., Coleman, R. and Minster, J.B. (2008), ***An investigation into the forces that drive ice-shelf rift propagation on the Amery Ice Shelf, East Antarctica***, *Journal of Glaciology*, vol. 54, no. 184, pp. 17-27.

Braun, M., Humbert, A. and Moll, A. (2009), ***Changes of Wilkins Ice Shelf over the past 15 years and inferences on its stability***, *The Cryosphere*, vol. 3, no. 1, pp. 41-56.

Brunner, F.K., Coleman, R. and Hirsch, B. (1981), ***A comparison of computation methods for crustal strains from geodetic measurements***, *Tectonophysics*, vol. 71, pp. 281-298.

Budd, W. (1966), ***The dynamics of the Amery Ice Shelf***, *Journal of Glaciology*, vol. 6, no. 45, pp. 335-358.

Budd, W.F., Corry, M.J. and Jacka, T.H. (1982), ***Results from the Amery Ice Shelf project***, *Annals of Glaciology*, vol. 3, pp. 36-41.

Budd, W., Landon Smith, I. and Wishart, E. (1967), ***The Amery Ice Shelf***, in H. Oura (ed) *The physics of snow and ice*, Proc. Int. Conf. on Low Temperature Science, Sapporo, Japan, Hokkaido University, Sapporo, pp. 447-467.

CSRS-PPP (2008), ***CSRS-PPP (Precise Point Positioning) service***, http://ess.nrcan.gc.ca/2002_2006/gnd/csrs_e.php (accessed July 21, 2009).

De Angelis, H. and Skvarca, P. (2003), ***Glacier surge after ice shelf collapse***, *Science*, vol. 299, no. 5612, pp. 1560-1562.

Fricker, H.A., Bassis, J.N., Minster, B. and MacAyeal, D.R. (2005a), ***ICESat's new perspective on ice shelf rifts: The vertical dimension***, *Geophysical Research Letters*, vol. 32**,** no. 23, L23S08, doi:10.1029/2005GL025070.

Fricker, H.A., Young, N.W., Allison, I. and Coleman, R. (2002), ***Iceberg calving from the Amery Ice Shelf, East Antarctica***, *Annals of Glaciology*, vol. 34, pp. 241-246.

Fricker, H.A., Young, N.W., Coleman, R., Bassis, J.N. and Minster, J.B. (2005b), ***Multi-year monitoring of rift propagation on the Amery Ice Shelf, East Antarctica***, *Geophysical Research Letters*, vol. 32, no. 2, L02502, doi:10.1029/2004GL021036.

Iz, H.B. (2006), ***Differencing reveals hidden changes in baseline length time-series***, *Journal of Geodesy*, vol. 80, no. 5, pp. 259-269.

Jacobs, S., Helmer, H., Doake, C., Jenkins, A. and Frolich, R. (1992), ***Melting of the ice shelves and the mass balance of Antarctica***, *Journal of Glaciology*, vol. 38, no. 130, pp. 375-387.

Janssen, V. (2009), ***Detection of abrupt baseline length changes using cumulative sums***, *Journal of Applied Geodesy*, vol. 3, no. 2, pp. 89-96.

Janssen, V., Coleman, R. and Bassis, J.N. (2009), ***GPS-derived strain rates on an active ice shelf rift***, *Survey Review*, vol. 41, no. 311, pp. 14-25.

Joughin, I. and MacAyeal, D.R. (2005), ***Calving of large tabular icebergs from ice shelf rift systems***, *Geophysical Research Letters*, vol. 32, no. 2, L02501, doi:10.1029/2004GL020978.

King, M. (2002), ***The dynamics of the Amery Ice Shelf from a combination of terrestrial and space geodetic data***, Ph.D. thesis, University of Tasmania, Hobart, Australia.

King, M. (2004), ***Rigorous GPS data processing strategies for glaciological applications***, *Journal of Glaciology*, vol. 50, no. 171, pp. 601-607.

King, M., Coleman, R. and Morgan, P. (2000), ***Treatment of horizontal and vertical tidal signals in GPS data: A case study on a floating ice shelf***, *Earth Planets Space*, vol. 52, no. 11, pp. 1043-1047.

Mercer, J.H. (1978), ***West Antarctic ice sheet and CO_2 greenhouse effect: A threat of disaster***, *Nature*, vol. 271, no. 5643, pp. 321-325.

Padman, L., Fricker, H.A., Coleman, R., Howard, S. and Erofeeva, L. (2002), ***A new tide model for the Antarctic ice shelves and seas***, *Annals of Glaciology*, vol. 34, pp. 247-254.

Rignot, E., Casassa, G., Gogineni, P., Krabill, W., Rivera, A. and Thomas, R. (2004), ***Accelerated ice discharge from the Antarctic Peninsula following the collapse of Larsen B ice shelf***, *Geophysical Research Letters*, vol. 31, no. 18, L18401, doi:10.1029/2004GL020697.

Rott, H., Rack, W., Skvarca, P. and De Angelis, H. (2002), ***Northern Larsen Ice Shelf, Antarctica: Further retreat after collapse***, *Annals of Glaciology*, vol. 34, pp. 277-282.

Scambos, T., Hulbe, C. and Fahnestock, M. (2003), ***Climate-induced ice shelf disintegration in the Antarctic Peninsula***, in E.W. Domack et al. (eds) *Antarctic Peninsula climate variability: A historical and paleoenvironmental perspective*, AGU, Washington DC, Antarctic Research Series, vol. 79, pp. 79-92.

Shepherd, A., Wingham, D. and Rignot, E. (2004), ***Warm ocean is eroding West Antarctic ice sheet***, *Geophysical Research Letters*, vol. 31, no. 23, L23402, doi:10.1029/2004GL021106.

USGS (2009), ***SLC-off products: Background***, http://landsat.usgs.gov/products_slcoffbackground.php (accessed July 21, 2009).

Vaughan, D.G. and Doake, C.S.M. (1996), ***Recent atmospheric warming and retreat of ice shelves on the Antarctic Peninsula***, *Nature*, vol. 379, no. 6563, pp. 328-331.

Young, N.W. and Hyland, G. (2002), ***Velocity and strain rates derived from InSAR analysis over the Amery Ice Shelf, East Antarctica***, *Annals of Glaciology*, vol. 34, no. 1, pp. 228-234.

Zhang, X. and Andersen, O.B. (2006), ***Surface ice flow velocity and tide retrieval of the Amery Ice Shelf using precise point positioning***, *Journal of Geodesy*, vol. 80, no. 4, pp. 171-176.

The corresponding author

Dr. Volker Janssen (Volker.Janssen@lpma.nsw.gov.au) holds a Dipl.-Ing. in Surveying from the University of Bonn, Germany, and a Ph.D. in GPS for volcano deformation monitoring from the University of New South Wales (UNSW). He worked as an assistant lecturer at UNSW and as graduate surveyor in Sydney before being a Lecturer in Surveying and Spatial Sciences at the University of Tasmania between 2004 and 2009. He is now a GNSS Surveyor (CORS Network) in the Survey Infrastructure and Geodesy branch at the NSW Land and Property Management Authority in Bathurst, Australia, where he is part of the team that operates the CORSnet-NSW network which covers Sydney and is currently being expanded to provide state-wide coverage. His research interests are in the fields of geodesy and geodynamics, with an emphasis on GPS/GNSS studies and CORS networks.